Interface Modification of ZnO-Based Inverted PTB7:$PC_{71}BM$ Organic Solar Cells by Cesium Stearate and Simultaneous Enhancement of Device Parameters

Guojie Wang,[†,‡] Tonggang Jiu,[*,†] Gang Tang,[†] Jun Li,[†] Pandeng Li,[†] Xiaojin Song,[‡] Fushen Lu,[‡] and Junfeng Fang[*,†]

[†]Institute of New Energy Technology, Ningbo Institute of Material Technology and Engineering (NIMTE), Chinese Academy of Science (CAS), Ningbo, Zhejiang 315201, P. R. China

[‡]Department of Chemistry, College of Science, Shantou University, Shantou, Guangdong 515063, P. R. China

Supporting Information

ABSTRACT: We used cesium stearate (CsSt) to modify the interface of the electron-extracting contact in inverted organic solar cells. Surface microstructure, optical properties, and electrical characterization as well as exciton generation rate and dissociation probability were investigated to understand the impact of CsSt on the interface contact. The results indicated that by incorporation of CsSt, the surface morphology and energy level as well as conductivity of a zinc oxide (ZnO) film were improved. On the basis of the above properties, highly efficient inverted organic solar cells have been demonstrated by using a ZnO nanoparticle film and CsSt stacked bilayer structure as the cathode interfacial layer. The insertion of a CsSt layer between the ZnO film and active layer improved the electron extraction efficiency, and a high power conversion efficiency (PCE) of 8.69% was achieved. The PCE was improved by 20% as compared to the reference device using a ZnO-only electron extraction layer.

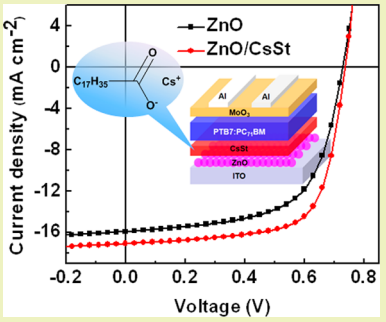

KEYWORDS: *Cesium stearate, Interfacial modification, Organic solar cells, Exciton dissociation*

INTRODUCTION

Solution-processed bulk heterojunction (BHJ) organic solar cells (OSCs) have attracted tremendous interest for applications in renewable energy because of their advantages of being low cost and lightweight and having easy fabrication and the capability to fabricate flexible large-area devices.[1−5] With the development of materials design and fabrication processes, the power conversion efficiency (PCE) of BHJ OSCs has been remarkably improved.[6−10] Recently, great improvements have been achieved such as the certified PCE of 9.2% for single-junction and 10.6% for tandem solar cells.[11,12] In addition, a PCE of more than 8% has also been reported in the small molecular solar cells.[13−15] Interfacial layers, located between the photoactive layer and electrodes, can significantly improve the performance of OSCs.[16−20] Such interfacial layers can be multifunctional materials that act as selective charge injection layers or modify electrodes, so that they can block charges from recombination at the active layer−electrode interfaces.[21−23] However, the lack of understanding of interface modification and impact of surface properties limit their further specification and development.[24−26] Therefore, developing new and more effective interfacial layers and investigating the interfacial property are vital for enhancing solar cell performance.

A thin film of n-type semiconducting zinc oxide (ZnO) nanoparticles is commonly used as an effective electron extraction layer in inverted OSCs owing to its high electron mobility and optical transparency, as well as its ease of processability.[27−29] However, the major challenge in employing ZnO nanoparticle film as an electron extraction layer is the presence of defects on the surface.[30] The surface defects allow the increased recombination of electrons and holes generated in the active layer.[27] In addition, sol−gel ZnO as an alternative was also reported for the electron extraction layer.[30−34] Sol−gel ZnO films are formed by annealing zinc acetate at high temperature. Therefore, colloidal ZnO nanoparticle film is the choice for electron extraction in OSCs due to its low temperature processing capability. Recently, a fullerene derivative,[32,33,35] poly(ethylene glycol) (PEG),[28,36] conjugated polyelectrolytes,[7,37,38] or poly(ethylene oxide) (PEO),[39,40] was widely designed and prepared to optimize the contact between ZnO and the active layer. However, the tedious synthesis and batch-to-batch variation of the polymer modifier might be the drawback for their application. In this sense, it is necessary to develop a ZnO nanoparticle film with low defects so as to further enhance the performance of inverted solar cells.

Cesium stearate (CsSt), consisting of an inorganic metallic cation and a long aliphatic hydrocarbon chain, is thought to be a promising interface modification material. It possesses both the properties of inorganic and organic materials and is expected to exhibit better interfacial compatibilities and

electronic properties. In this work, we employed CsSt as an interfacial modification material and studied the effects of CsSt on the interface property and device performance in OSCs devices. The changes in surface microstructure and optical and electrical properties as well as exciton generation rate and dissociation probability were analyzed to investigate the mechanism of interfacial improvement. After incorporation of a thin CsSt layer onto the ZnO nanoparticle film, the surface traps of ZnO film were passivated, and the film morphology was improved. The interface improvement gave a power conversion efficiency of 8.69% and significantly enhanced the performance of OSCs over that of a ZnO-based device by 20%. Such treatment can also prevent a direct contact of the active layer with ZnO and therefore further reduce the recombination of electron and hole on the surface of ZnO films.

RESULTS AND DISCUSSION

The device architecture of inverted OSCs and the energy level diagram of materials are illustrated in Figure 1. The device

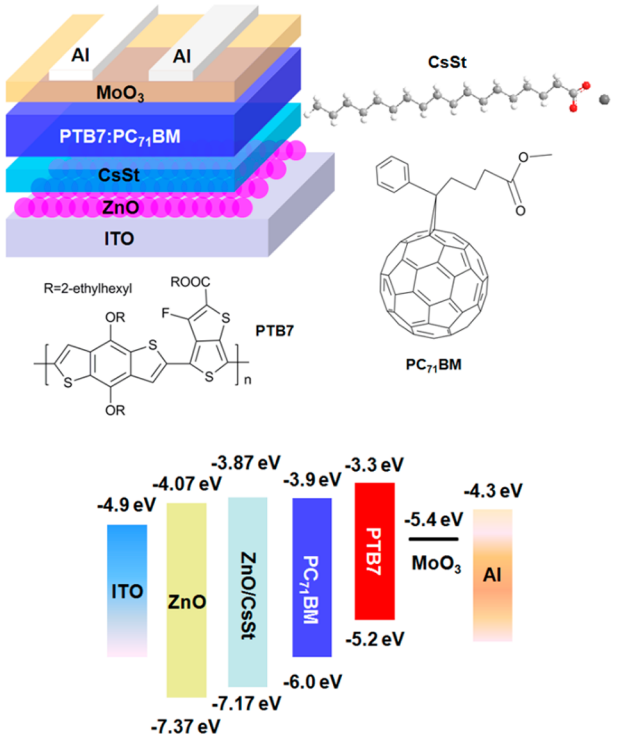

Figure 1. Schematic illustration of the inverted device architecture and the chemical structure and energy level of the materials used in the work.

consisted of ITO/ZnO/CsSt film/polymer active layer/MoO_3/Al. For the photoactive layer materials, we used poly[[4,8-bis[(2-ethylhexyl)oxy]benzo-[1,2-b:4,5-b′]dithiophene-2,6-diyl][3-fluoro-2-[(2-ethylhexyl)-carbonyl]-thieno-[3,4-*b*]-thiophenediyl]] (PTB7) as the donor material and [6,6]-phenyl-C_{71}-butyric acid methyl ester ($PC_{71}BM$) as the acceptor material. For comparison, the device with the ZnO-only interfacial layer was also fabricated.

To investigate the effect of CsSt on the surface morphology of interfacial layer, a scanning electron microscope (SEM) and atomic force microscope (AFM) were employed, and the results are shown in Figure 2. The presence of voids was observed in the ZnO surface (Figure 2a), which was improved

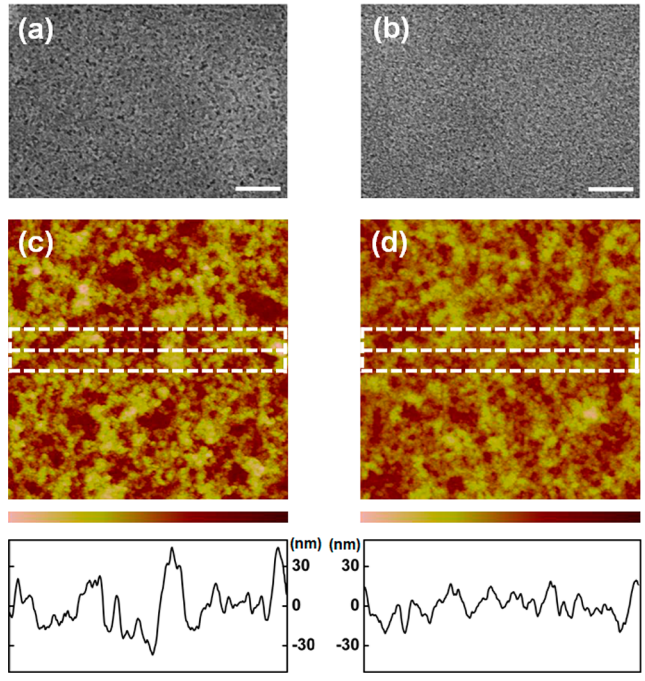

Figure 2. SEM images of (a) ZnO and (b) ZnO/CsSt films (scale bar is 200 nm). AFM height images and surface profiles of (c) ZnO and (d) ZnO/CsSt interfacial layers with a scan size of 5 μm × 5 μm.

and became continuous and uniform after the spin-casting of CsSt (Figure 2b). In Figure 2c, the AFM height image showed that the ZnO nanoparticle film exhibited a root-mean-square (RMS) roughness of 28.7 nm at a scan scale of 5 μm × 5 μm. On the other hand, when the ZnO film was covered by CsSt, the surface became smoother with a RMS roughness of 21.2 nm (Figure 2d), indicating that the voids between the ZnO nanoparticles were partially filled by CsSt and the film was planarized. The interface traps increased the possibility of trap-assisted recombination of the electron, leading to the low fill factor (FF) of device. The smooth film has fewer traps, which decrease this recombination possibility. Hence, the reduced roughness of the ZnO film could contribute to increasing FF. An AFM measurement was also employed to investigate the morphology of the active layer. The RMS roughness of the active layer on the ZnO film was 9.6 nm, which was higher than that (7.0 nm) on the ZnO/CsSt film (Figure S1, Supporting Information). Obviously, the roughness of the substrate could affect the roughness of the active layer spin-casting on it. The rough active layer was unfavorable for device performance. The influence of CsSt on the electric property of the interlayer was measured by the conductive AFM measurement (Figure S2, Supporting Information); the current RMS of ZnO film was 14.6 nA. When it was covered by a CsSt layer, the current RMS (4.1 nA) was decreased. The lower RMS current implied that the surface electrical conductivity was more uniformly distributed.[18,42] While there was some resistance contribution from the lower conductivity in the ZnO/CsSt case, the reduction of current RMS should counteract the effects of the low conductance. Additionally, these results implied the importance of using a relatively thin CsSt layer to reduce resistance effects.

The passivation effect on the ZnO film was investigated by photoluminescence (PL) measurements. As shown in Figure 3, ZnO has two emission peaks, a near band-edge emission at 373

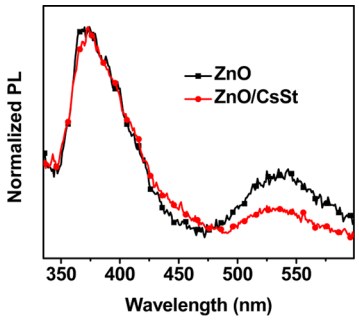

Figure 3. Photoluminescence spectra of the ZnO nanoparticle film with and without the CsSt layer.

nm and a deep level emission by surface defects at 535 nm.[27,43] The PL spectra of ZnO were normalized by the emission intensity of the near band-edge at 373 nm.[39,42] The PL intensity at 535 nm, corresponding to the trap emission, decreased after insertion of a CsSt layer, indicating that the surface defects were restrained and repaired by modification with CsSt (Figure 3).[28,30,36] In the photovoltaic device, the reduction of traps can decrease the possibility of trap-assisted interfacial recombination of carriers and consequently enhance short-circuit current density (J_{sc}) and FF of the device; thus, the PCE of device was improved. The UV–vis transmission spectrum of the ZnO/CsSt layer is shown in Figure S3 of the Supporting Information. The ZnO/CsSt layer only absorbed UV light and was transparent in the visible range. This indicated that visible light was allowed to pass through it and irradiate into the active layer. In the meantime, the photodegradation of the polymer active layer induced by UV light was reduced.

To investigate the effect of CsSt on the electronic property, ultraviolet photoelectron spectroscopy (UPS) was carried out to study the electronic energy levels (highest occupied molecular orbital (HOMO) and lowest unoccupied molecular orbital (LUMO) levels) of the interfacial layer (Figure 4 and

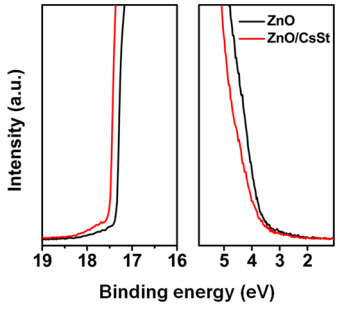

Figure 4. UPS spectra of ZnO and ZnO/CsSt film on ITO glass substrates.

Table S1, Supporting Information). The ZnO film shows a photoemission cutoff at 17.33 eV, which corresponds to a work function (WF) of 3.87 eV. After spin-casting the CsSt layer, the WF value decreases to 3.71 eV. A 0.16 eV shift indicates a lowering of the WF of ZnO, leading to a downward vacuum level shift. Thus, the modification of a high WF ZnO surface to a lower WF surface is beneficial for enhancing the built-in potential in devices, which in turn contributed to the enhanced V_{oc} and the electron collection to the cathode.[36] The HOMO level (7.17 eV) of the ZnO/CsSt was lowered by 0.2 eV relative to the HOMO level (7.37 eV) of ZnO. The LUMO levels of ZnO and ZnO/CsSt can be determined as 4.07 eV (ZnO) and 3.87 eV (ZnO/CsSt) by subtracting the optical bandgap (3.3 eV for both cases), as derived from UV absorption result (Figure S4, Supporting Information). The difference in LUMO energy levels between ZnO and ZnO/CsSt showed that the LUMO energy level of ZnO was tuned by the CsSt thin layer. The results implied that the incorporation of CsSt formed an intermediate energy gradient at the interface between the interlayer and active layer, which facilitated the electron transfer to the ITO cathode.[32,33]

To investigate the impact of CsSt on the performance of the solar cells, the inverted OSCs device was test. The current density–voltage (J–V) curves under illumination and in the dark with ZnO-only, the ZnO/CsSt bilayer, and CsSt-only as interfacial layers are shown in Figure 5. The photovoltaic device

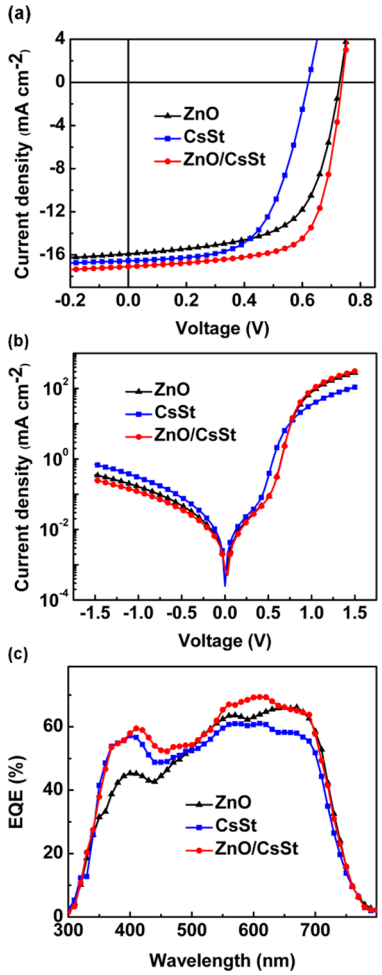

Figure 5. Current density–voltage (J–V) characteristics of the devices with ZnO, CsSt, or ZnO/CsSt as the interfacial layers measured (a) under illumination and (b) in the dark. (c) EQE spectra of solar cells with a ZnO, CsSt, and ZnO/CsSt interfacial layers.

parameters of open-circuit voltage (V_{oc}), J_{sc}, FF, and PCE are summarized in Table 1. The reference device based on ZnO exhibited a PCE of 7.22%, with V_{oc} of 0.729 V, J_{sc} of 15.88 mA cm^{-2}, and FF of 62.4%. When CsSt alone was used as an interfacial layer, the J_{sc} of the device was 16.54 mA cm^{-2}, but the V_{oc} and FF dropped to 0.620 V and 60.1%, respectively. After depositing the CsSt layer onto the ZnO film to reengineer the interface, the device showed an enhanced V_{oc} of 0.736 V, J_{sc}

Table 1. V_{oc}, J_{sc}, FF, and PCE of Various Inverted Devices with Different Interfacial Layers

				PCE (%)	
devices	V_{oc} (V)	J_{sc} (mA cm^{-2})	FF (%)	best	average
ZnO	0.729	15.88	62.4	7.22	6.97
CsSt	0.620	16.54	60.1	6.16	5.95
ZnO/CsSt	0.736	17.07	69.1	8.69	8.46

of 17.07 mA cm^{-2}, and FF of 69.1% and hence showed a remarkably enhanced PCE of 8.69% in comparison with the reference devices. In order to check the reproducibility of the device, six devices using the ZnO/CsSt bilayer as the interfacial layer were examined under the same conditions. The maximum and average PCE were 8.69% and 8.46%, respectively, which suggested the device could present excellent performance and favorable reproducibility by using the ZnO/CsSt stacked bilayer structure as the cathode interfacial layer. Moreover, the inverted OSCs with a ZnO/CsSt interfacial layer were optimized, and the optimized concentration of CsSt was 1 mg mL^{-1}, as shown in Figure S5 and Table S2 of the Supporting Information. To further scrutinize the electrical characteristics of the device, the J–V curves of the devices with ZnO/CsSt interfacial layers in the dark are presented in Figure 5b. Evidently, the control device showed a high leakage current in the reverse direction. However, the ZnO/CsSt-based device exhibited excellent diode characteristics with a lower leakage current, which was favorable for electron extraction. Figure 5c shows the external quantum efficiency (EQE) spectra of the device based on the ZnO and ZnO/CsSt interlayers. The device with CsSt exhibited a substantial enhancement response from the wavelength range of 340–650 nm as compared with that of the ZnO-only interlayer, which leads to a large forward current J_{sc} as shown in Figure 5a. This indicated that the interface between the active layer and ITO/ZnO was improved by inserting the CsSt layer. To study the effects of the CsSt on the device stability, we performed a side-by-side comparison of the lifetime between non-encapsulated ZnO- and ZnO/CsSt-based devices stored in an argon filled glovebox. Figure 6 shows the normalized

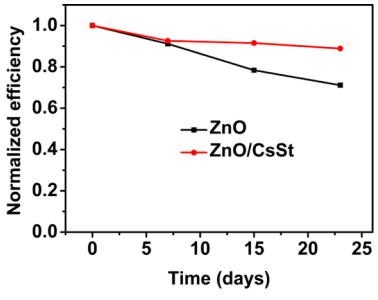

Figure 6. Normalized device performance as a function of storage time based on ZnO and ZnO/CsSt interfacial layers. Devices were stored in an argon filled glovebox without encapsulation.

efficiency of the devices versus storage time. As the data shows, the ZnO/CsSt-based device degraded slower than the ZnO-only device did within 23 days. This indicated that the device lifetime was improved by the modification of CsSt.

To further illustrate the effect of CsSt on the performance of the solar cells, we determine the maximum exciton generation rate (G_{max}) and exciton dissociation probability (P) in the devices. Figure 7 reveals the effect of the bilayer structure on

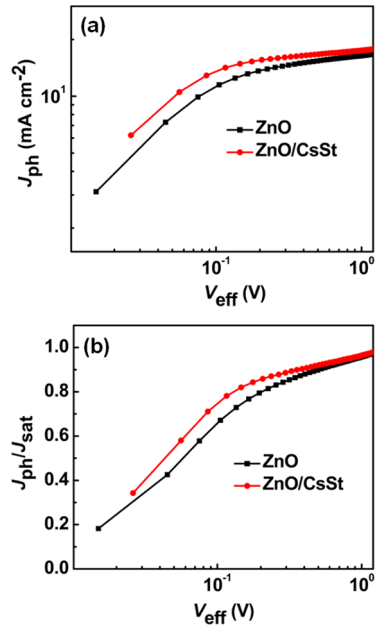

Figure 7. (a) Plots of photocurrent density (J_{ph}) with respect to the effective bias (V_{eff}) in the devices with ZnO or ZnO/CsSt as the interfacial layers. (b) Corresponding plots of J_{ph}/J_{sat} with respect to the effective bias (V_{eff}) in the two devices.

the photocurrent density (J_{ph}) versus the effective voltage (V_{eff}). J_{ph} is calculated as $J_{ph} = J_L - J_D$, where J_L and J_D are the current density under illumination and in the dark, respectively. V_{eff} is determined as $V_{eff} = V_0 - V_a$, where V_0 is the voltage at which J_{ph} is zero and V_a is the applied voltage.[44–46] Figure 7a clearly showed that J_{ph} increased at a low V_{eff} range for both devices and was saturated at a high V_{eff} (1.5 V). It suggested that all the photogenerated excitons dissociated into free charge carriers and were collected at the electrodes. In this case, saturation current density (J_{sat}) is only limited by the amount of absorbed incident photons. Thus, the G_{max} could be given from $J_{sat} = qG_{max}L$, where q is the electronic charge and L is the thickness of active layer (110 nm).[45,46] The values of G_{max} for the ZnO-only and ZnO/CsSt devices are 9.72 × 10^{27} m^{-3} s^{-1} (J_{sat} = 171.2 A m^{-2}) and 10.29 × 10^{27} m^{-3} s^{-1} (J_{sat} = 181.3 A m^{-2}), respectively. An enhancement of G_{max} occurred after incorporation of the CsSt layer onto the ZnO film. The P values can be obtained from the ratio of J_{ph}/J_{sat} (Figure 7b). We can see that exciton dissociation probability of the device with the ZnO/CsSt bilayer is higher than that of the device with the ZnO-only across the full range. P values under the J_{sc} condition increase from 92.9% in the ZnO-only device to 94.2% in the device with the ZnO/CsSt-stacked bilayer structure. Interestingly, in the low effective voltage range, the P values for the two devices show large differences. For example, at 0.2 V of V_{eff}, P is 79.5% for the device with the ZnO-only interlayer, while it is 85.7% for the device with the ZnO/CsSt-stacked bilayer structure interlayer. Because the P value is the exciton dissociation efficiency, a lower P value indicates reduced exciton dissociation efficiency. It suggests that exciton recombination begins to dominate the process and thus leads to a lower fill factor in the device without the CsSt layer.[47] The J_{ph}–V_{eff} characteristics from the device with the bilayer interfacial layer identify the effect of CsSt on reducing the exciton recombination and benefiting the dissociation of excitons into free charge carriers at a low effective voltage. An increase in the exciton dissociation

probability reduces the recombination rate of excitons and therefore improved the PCE of OSCs.

CONCLUSION

In this work, we showed that modifying the interface between ZnO and the photoactive layer with CsSt can improve the OSCs performance effectively. SEM and AFM including C-AFM characterization showed that CsSt modification to the ZnO nanoparticle film can effectively modify the film morphology and electric property. PL spectra indicated that the CsSt passivates the surface traps of the ZnO film, which can decrease the possibility of trap-assisted interfacial recombination of the carriers. This was also verified by exiton generation rate (G_{max}) and dissociation probability (P) measurement. Consequently, V_{oc}, J_{sc}, and FF of the inverted solar cells were considerably improved. The PCE of the device therefore with the PTB7:$PC_{71}BM$ photoactive layer was significantly improved from the original 7.22% to 8.69%. These results indicated that the applicable CsSt layer could be applied as the electron-contact modifier layer for high-efficiency inverted polymer solar cell.

EXPERIMENTAL METHODS

Materials. Indium tin oxide (ITO)-coated glass substrates were purchased from Shenzhen Nan Bo Group, China. Electron donor material poly[[4,8-bis[(2-ethylhexyl)oxy]benzo-[1,2-b:4,5-b′]-dithiophene-2,6-diyl][3-fluoro-2-[(2-ethylhexyl)-carbonyl]-thieno-[3,4-*b*]thiophenediyl]] (PTB7) and electron acceptor material [6,6]-phenyl-C_{71}-butyric acid methyl ester ($PC_{71}BM$) were purchased from 1-Material Chemscitech and ADS, respectively. Chlorobenzene and 1,8-diiodoctane were provided by Sigma-Aldrich. Cs_2CO_3, stearic acid and *n*-butanol were purchased from Sinopharm Chemical Reagent Co., Ltd. All these commercially available chemicals were used as received. Cesium stearate was synthesized according to the previous report.[41] Briefly, Cs_2CO_3 and stearic acid (1:2 molar ratio) were added to *n*-butanol and kept reflux until no more CO_2 formed. Subsequently, *n*-butanol was separated on the rotary evaporator. The residue was mixed with diethyl ether and aspirated. Zinc oxide nanoparticles were prepared using an adapted procedure from the literatures.[12,48] Briefly, 2.95 g of zinc acetate dihydrate was dissolved in 125 mL of methanol at 60 °C under vigorous stirring. A solution of KOH (1.48 g) in methanol (65 mL) was dropped into the zinc acetate dihydrate solution in 10 min under vigorous stirring. The solution temperature was held at 60 °C and stirred for 2 h and 15 min, and then, the heater and stirrer were removed to allow the nanoparticles to precipitate for an additional 2 h. Precipitate and mother liquor were separated, and the precipitate was washed with 50 mL of methanol for 10 min. The suspension was centrifuged to collect the nanoparticles.

Device Fabrication. The device structure was ITO/ZnO/CsSt/PTB7:$PC_{71}BM$/MoO_3/Al. The ITO substrates were cleaned by sequential ultrasonic treatment in detergent, deionized water, acetone, and isopropanol for 30 min, respectively. Then, they were blown dry with nitrogen. Subsequently, the substrates were moved into an ultraviolet chamber for UV−ozone treatment for 20 min. The ZnO nanoparticles were dissolved in chloroform, and the solution with a concentration of 15 mg/mL was spin-coated at 1500 rpm for 60 s on the ITO substrates and then annealed at 80 °C for 10 min. The film thickness is 30 nm. Next, cesium stearate in methanol with a different concentration was spin-coated at 4000 rpm for 60 s on the top of the ZnO film and annealed at 80 °C for 10 min. The thickness of CsSt on the ZnO nanoparticle film is too thin to measure. All substrates were then transferred to the argon-filled glovebox for further processing. Electron donor material PTB7 and electron acceptor material $PC_{71}BM$ (10:15 wt/wt) were weighed (total concentration is 25 mg mL^{-1}) and dissolved in mixed solvents of chlorobenzene/1,8-diiodoctane (97:3% by volume) in the argon-filled glovebox. The solution was stirred at 60 °C for a minimum of 12 h and spin-coated on the freshly prepared ZnO/CsSt interlayer at 2000 rpm for 120 s in the glovebox. The thickness of the active layer was around 110 nm. The device fabrication was completed after thermal evaporation of 10 nm of MoO_3 and 100 nm of Al under vacuum at a base pressure of about 1×10^{-6} Torr. A shadow mask was used during the thermal evaporation to define the device area of 0.04 cm^2.

Measurements and Characterization. The current density−voltage characteristics of the photovoltaic devices were recorded using a computer-controlled Keithley 2400 source meter under 1 sun, AM 1.5G, simulated solar light. The measurement of external quantum efficiency (EQE) was performed using a IQE200TM data acquisition system. Scanning electron microscopy (SEM) images were conducted on a S-4800 scanning electron microscope operated at an acceleration voltage of 4 kV. Atomic force microscopy (AFM) was used to measure film roughness and surface morphologies in tapping mode using a Veeco dimension V atomic microscope. The AFM cantilever coated with Pt/Ir was employed for conductive AFM measurements, and contact mode was selected. The transmittance spectra were recorded on a UV-3300 spectrophotometer. UPS was performed using a Kratos AXIS ULTRA^{DLD} UPS/XPS system (Kratos analytical, Manchester, U.K.). UPS was carried out using He I radiation at 21.2 eV from a discharge lamp operated at 20 mA, a pass energy of 5 eV, and a channel width of 25 meV.

ASSOCIATED CONTENT

Supporting Information

AFM height images and surface profiles of the PTB7:$PC_{71}BM$ active layer on the ZnO and ZnO/CsSt interfacial layers, conductive AFM images of ZnO and the ZnO/CsSt interfacial layer, transmission spectra of ZnO and ZnO/CsSt film on ITO glass substrates, UV−vis absorption spectra of ZnO and ZnO/CsSt on quartz, current density−voltage (*J-V*) characteristics of the devices with different concentrations of CsSt spin-coated on ZnO film as an interfacial layer under illumination and in the dark, and distribution and statistical analysis of the devices parameters. This material is available free of charge via the Internet at http://pubs.acs.org.

AUTHOR INFORMATION

Corresponding Authors

*E-mail: jiutonggang@nimte.ac.cn (T.J.).
*E-mail: fangjf@nimte.ac.cn (J.F.).

Notes

The authors declare no competing financial interests.

ACKNOWLEDGMENTS

The authors gratefully acknowledge the support of the National Natural Science Foundation of China (51202264, 51273208, and 51272152) and the Specialized Research Fund for the Spring Buds Talent Program (Y20804RA02). The work was also supported by Hundred Talent Program of Chinese Academy of Science, Guangdong Natural Science Foundation (S2013010014171).

REFERENCES

(1) Dang, M. T.; Hirsch, L.; Wantz, G.; Wuest, J. D. Controlling the morphology and performance of bulk heterojunctions in solar cells. Lessons learned from the benchmark poly(3-hexylthiophene):[6,6]-phenyl-c_{61}-butyric acid methyl ester system. *Chem. Rev.* **2013**, *113*, 3734−3765.

(2) Li, W.; Furlan, A.; Hendriks, K. H.; Wienk, M. M.; Janssen, R. A. J. Efficient tandem and triple-junction polymer solar cells. *J. Am. Chem. Soc.* **2013**, *135*, 5529−5532.

(3) Kaltenbrunner, M.; White, M. S.; Głowacki, E. D.; Sekitani, T.; Someya, T.; Sariciftci, N. S.; Bauer, S. Ultrathin and lightweight organic solar cells with high flexibility. *Nat. Commun.* **2012**, *3*, 770.
(4) Graetzel, M.; Janssen, R. A. J.; Mitzi, D. B.; Sargent, E. H. Materials interface engineering for solution-processed photovoltaics. *Nature* **2012**, *488*, 304−312.
(5) Yang, L.; Yan, L.; You, W. Organic solar cells beyond one pair of donor−acceptor: Ternary blends and more. *J. Phys. Chem. Lett.* **2013**, *4*, 1802−1810.
(6) Zhou, H.; Zhang, Y.; Seifter, J.; Collins, S. D.; Luo, C.; Bazan, G. C.; Nguyen, T.-Q.; Heeger, A. J. High-efficiency polymer solar cells enhanced by solvent treatment. *Adv. Mater.* **2013**, *25*, 1646−1652.
(7) Yang, T.; Wang, M.; Duan, C.; Hu, X.; Huang, L.; Peng, J.; Huang, F.; Gong, X. Inverted polymer solar cells with 8.4% efficiency by conjugated polyelectrolyte. *Energy Environ. Sci.* **2012**, *5*, 8208−8214.
(8) Seo, J. H.; Gutacker, A.; Sun, Y.; Wu, H.; Huang, F.; Cao, Y.; Scherf, U.; Heeger, A. J.; Bazan, G. C. Improved high-efficiency organic solar cells via incorporation of a conjugated polyelectrolyte interlayer. *J. Am. Chem. Soc.* **2011**, *133*, 8416−8419.
(9) Lu, L.; Luo, Z.; Xu, T.; Yu, L. Cooperative plasmonic effect of ag and au nanoparticles on enhancing performance of polymer solar cells. *Nano Lett.* **2013**, *13*, 59−64.
(10) Liu, S.; Zhang, K.; Lu, J.; Zhang, J.; Yip, H.-L.; Huang, F.; Cao, Y. High-efficiency polymer solar cells via the incorporation of an amino-functionalized conjugated metallopolymer as a cathode interlayer. *J. Am. Chem. Soc.* **2013**, *135*, 15326−15329.
(11) He, Z.; Zhong, C.; Su, S.; Xu, M.; Wu, H.; Cao, Y. Enhanced power-conversion efficiency in polymer solar cells using an inverted device structure. *Nat. Photonics* **2012**, *6*, 591−595.
(12) You, J.; Dou, L.; Yoshimura, K.; Kato, T.; Ohya, K.; Moriarty, T.; Emery, K.; Chen, C.-C.; Gao, J.; Li, G.; Yang, Y. A polymer tandem solar cell with 10.6% power conversion efficiency. *Nat. Commun.* **2013**, *4*, 1446.
(13) Wang, D. H.; Kyaw, A. K. K.; Gupta, V.; Bazan, G. C.; Heeger, A. J. Enhanced efficiency parameters of solution-processable small-molecule solar cells depending on ITO sheet resistance. *Adv. Energy Mater.* **2013**, *3*, 1161−1165.
(14) Zhou, J.; Zuo, Y.; Wan, X.; Long, G.; Zhang, Q.; Ni, W.; Liu, Y.; Li, Z.; He, G.; Li, C.; Kan, B.; Li, M.; Chen, Y. Solution-processed and high-performance organic solar cells using small molecules with a benzodithiophene unit. *J. Am. Chem. Soc.* **2013**, *135*, 8484−8487.
(15) Kyaw, A. K. K.; Wang, D. H.; Wynands, D.; Zhang, J.; Nguyen, T.-Q.; Bazan, G. C.; Heeger, A. J. Improved light harvesting and improved efficiency by insertion of an optical spacer (ZnO) in solution-processed small-molecule solar cells. *Nano Lett.* **2013**, *13*, 3796−3801.
(16) Manders, J. R.; Tsang, S.-W.; Hartel, M. J.; Lai, T.-H.; Chen, S.; Amb, C. M.; Reynolds, J. R.; So, F. Solution-processed nickel oxide hole transport layers in high efficiency polymer photovoltaic cells. *Adv. Funct. Mater.* **2013**, *23*, 2993−3001.
(17) Xie, F.; Choy, W. C. H.; Wang, C.; Li, X.; Zhang, S.; Hou, J. Low-temperature solution-processed hydrogen molybdenum and vanadium bronzes for an efficient hole-transport layer in organic electronics. *Adv. Mater.* **2013**, *25*, 2051−2055.
(18) Wang, G.; Jiu, T.; Li, P.; Li, J.; Sun, C.; Lu, F.; Fang, J. Preparation and characterization of MoO_3 hole-injection layer for organic solar cell fabrication and optimization. *Sol. Energy Mater. Sol. Cells* **2014**, *120*, 603−609.
(19) Zacher, B.; Gantz, J. L.; Richards, R. E.; Armstrong, N. R. Organic solar cells—At the interface. *J. Phys. Chem. Lett.* **2013**, *4*, 1949−1952.
(20) Knesting, K. M.; Ju, H.; Schlenker, C. W.; Giordano, A. J.; Garcia, A.; Smith, O. N. L.; Olson, D. C.; Marder, S. R.; Ginger, D. S. ITO interface modifiers can improve VOC in polymer solar cells and suppress surface recombination. *J. Phys. Chem. Lett.* **2013**, *4*, 4038−4044.
(21) Po, R.; Carbonera, C.; Bernardi, A.; Camaioni, N. The role of buffer layers in polymer solar cells. *Energy Environ. Sci.* **2011**, *4*, 285−310.
(22) Yip, H.-L.; Jen, A. K. Y. Recent advances in solution-processed interfacial materials for efficient and stable polymer solar cells. *Energy Environ. Sci.* **2012**, *5*, 5994−6011.
(23) Kirchartz, T.; Agostinelli, T.; Campoy-Quiles, M.; Gong, W.; Nelson, J. Understanding the thickness-dependent performance of organic bulk heterojunction solar cells: The influence of mobility, lifetime, and space charge. *J. Phys. Chem. Lett.* **2012**, *3*, 3470−3475.
(24) Dibb, G. F. A.; Kirchartz, T.; Credgington, D.; Durrant, J. R.; Nelson, J. Analysis of the relationship between linearity of corrected photocurrent and the order of recombination in organic solar cells. *J. Phys. Chem. Lett.* **2011**, *2*, 2407−2411.
(25) Andersson, L. M.; Melianas, A.; Infahasaeng, Y.; Tang, Z.; Yartsev, A.; Inganäs, O.; Sundström, V. Unified study of recombination in polymer:fullerene solar cells using transient absorption and charge-extraction measurements. *J. Phys. Chem. Lett.* **2013**, *4*, 2069−2072.
(26) Lange, I.; Kniepert, J.; Pingel, P.; Dumsch, I.; Allard, S.; Janietz, S.; Scherf, U.; Neher, D. Correlation between the open circuit voltage and the energetics of organic bulk heterojunction solar cells. *J. Phys. Chem. Lett.* **2013**, *4*, 3865−3871.
(27) Chen, S.; Small, C. E.; Amb, C. M.; Subbiah, J.; Lai, T.-h.; Tsang, S.-W.; Manders, J. R.; Reynolds, J. R.; So, F. Inverted polymer solar cells with reduced interface recombination. *Adv. Energy Mater.* **2012**, *2*, 1333−1337.
(28) Jo, S. B.; Lee, J. H.; Sim, M.; Kim, M.; Park, J. H.; Choi, Y. S.; Kim, Y.; Ihn, S.-G.; Cho, K. High performance organic photovoltaic cells using polymer-hybridized ZnO nanocrystals as a cathode interlayer. *Adv. Energy Mater.* **2011**, *1*, 690−698.
(29) Boix, P. P.; Ajuria, J.; Etxebarria, I.; Pacios, R.; Garcia-Belmonte, G.; Bisquert, J. Role of ZnO electron-selective layers in regular and inverted bulk heterojunction solar cells. *J. Phys. Chem. Lett.* **2011**, *2*, 407−411.
(30) Small, C. E.; Chen, S.; Subbiah, J.; Amb, C. M.; Tsang, S.-W.; Lai, T.-H.; Reynolds, J. R.; So, F. High-efficiency inverted dithienogermole-thienopyrrolodione-based polymer solar cells. *Nat. Photonics* **2012**, *6*, 115−120.
(31) Kyaw, A. K. K.; Wang, D. H.; Gupta, V.; Zhang, J.; Chand, S.; Bazan, G. C.; Heeger, A. J. Efficient solution-processed small-molecule solar cells with inverted structure. *Adv. Mater.* **2013**, *25*, 2397−2402.
(32) Cheng, Y.-S.; Liao, S.-H.; Li, Y.-L.; Chen, S.-A. Physically adsorbed fullerene layer on positively charged sites on zinc oxide cathode affords efficiency enhancement in inverted polymer solar cell. *ACS Appl. Mater. Interfaces* **2013**, *5*, 6665−6671.
(33) Liao, S.-H.; Jhuo, H.-J.; Cheng, Y.-S.; Chen, S.-A. Fullerene derivative-doped zinc oxide nanofilm as the cathode of inverted polymer solar cells with low-bandgap polymer (PTB7-Th) for high performance. *Adv. Mater.* **2013**, *25*, 4766−4771.
(34) Yang, T.; Cai, W.; Qin, D.; Wang, E.; Lan, L.; Gong, X.; Peng, J.; Cao, Y. Solution-processed zinc oxide thin film as a buffer layer for polymer solar cells with an inverted device structure. *J. Phys. Chem. C* **2010**, *114*, 6849−6853.
(35) Cheng, Y.-J.; Hsieh, C.-H.; He, Y.; Hsu, C.-S.; Li, Y. Combination of -ndene-C60 bis-adduct and cross-linked fullerene interlayer leading to highly efficient inverted polymer solar cells. *J. Am. Chem. Soc.* **2010**, *132*, 17381−17383.
(36) Hu, T.; Li, F.; Yuan, K.; Chen, Y. Efficiency and air-stability improvement of flexible inverted polymer solar cells using ZnO/poly(ethylene glycol) hybrids as cathode buffer layers. *ACS Appl. Mater. Interfaces* **2013**, *5*, 5763−5770.
(37) Xie, C.; Chen, L.; Chen, Y. Electrostatic self-assembled metal oxide/conjugated polyelectrolytes as electron-transporting layers for inverted solar cells with high efficiency. *J. Phys. Chem. C* **2013**, *117*, 24804−24814.
(38) Chang, Y.-M.; Leu, C.-Y. Conjugated polyelectrolyte and zinc oxide stacked structure as an interlayer in highly efficient and stable organic photovoltaic cells. *J. Mater. Chem. A* **2013**, *1*, 6446−6451.

(39) Shao, S.; Zheng, K.; Pullerits, T.; Zhang, F. Enhanced performance of inverted polymer solar cells by using poly(ethylene oxide)-modified ZnO as an electron transport layer. *ACS Appl. Mater. Interfaces* **2013**, *5*, 380−385.
(40) Shao, S.; Zheng, K.; Zidek, K.; Chabera, P.; Pullerits, T.; Zhang, F. Optimizing ZnO nanoparticle surface for bulk heterojunction hybrid solar cells. *Sol. Energy Mater. Sol. Cells* **2013**, *118*, 43−47.
(41) Wetzelaer, G. A. H.; Najafi, A.; Kist, R. J. P.; Kuik, M.; Blom, P. W. M. Efficient electron injection from solution-processed cesium stearate interlayers in organic light-emitting diodes. *Appl. Phys. Lett.* **2013**, *102*, 053301.
(42) Kim, K.-D.; Lim, D. C.; Hu, J.; Kwon, J.-D.; Jeong, M.-G.; Seo, H. O.; Lee, J. Y.; Jang, K.-Y.; Lim, J.-H.; Lee, K. H.; Jeong, Y.; Kim, Y. D.; Cho, S. Surface modification of a ZnO electron-collecting layer using atomic layer deposition to fabricate high-performing inverted organic photovoltaics. *ACS Appl. Mater. Interfaces* **2013**, *5*, 8718−8723.
(43) Ischenko, V.; Polarz, S.; Grote, D.; Stavarache, V.; Fink, K.; Driess, M. Zinc oxide nanoparticles with defects. *Adv. Funct. Mater.* **2005**, *15*, 1945−1954.
(44) Shrotriya, V.; Yao, Y.; Li, G.; Yang, Y. Effect of self-organization in polymer/fullerene bulk heterojunctions on solar cell performance. *Appl. Phys. Lett.* **2006**, *89*, 063505.
(45) Chen, F.-C.; Wu, J.-L.; Lee, C.-L.; Hong, Y.; Kuo, C.-H.; Huang, M. H. Plasmonic-enhanced polymer photovoltaic devices incorporating solution-processable metal nanoparticles. *Appl. Phys. Lett.* **2009**, *95*, 013305.
(46) Xu, M.-F.; Zhu, X.-Z.; Shi, X.-B.; Liang, J.; Jin, Y.; Wang, Z.-K.; Liao, L.-S. Plasmon resonance enhanced optical absorption in inverted polymer/fullerene solar cells with metal nanoparticle-doped solution-processable TiO_2 layer. *ACS Appl. Mater. Interfaces* **2013**, *5*, 2935−2942.
(47) He, Z.; Zhong, C.; Huang, X.; Wong, W.-Y.; Wu, H.; Chen, L.; Su, S.; Cao, Y. Simultaneous enhancement of open-circuit voltage, short-circuit current density, and fill factor in polymer solar cells. *Adv. Mater.* **2011**, *23*, 4636−4643.
(48) Beek, W. J. E.; Wienk, M. M.; Kemerink, M.; Yang, X.; Janssen, R. A. J. Hybrid zinc oxide conjugated polymer bulk heterojunction solar cells. *J. Phys. Chem. B* **2005**, *109*, 9505−9516.